CHEMISTRY
A EUROPEAN JOURNAL

DOI: 10.1002/chem.200601811

High-Efficiency Electrophosphorescent Copolymers Containing Charged Iridium Complexes in the Side Chains

Bin Du, Lei Wang, HongBin Wu, Wei Yang,* Yong Zhang, RanSheng Liu, MingLiang Sun, Junbiao Peng,* and Yong Cao[a]

Abstract: A convenient approach to novel charged Ir polymers for optoelectronic devices to achieve red emission was developed. 2-(Pyridin-2-yl)-benzimidazole units grafted into the side chains of macroligands (PFCz and PFP) served as ligands for the formation of charged Ir complex pendants with 1-phenylisoquinoline (1-piq). The charged Ir polymers (PFPIrPiq and PFCzIrPiq) showed exclusive $Ir(1\text{-piq})_2\{N\text{-}[2\text{-(pyridin-2-yl)benzimidazole]hexyl}\}^+BF_4^-$ (IrPiq) emission, with the peak at 595 nm. The best device performances were obtained from PFCzIrPiq4 with the device configuration of ITO/PEDOT:PSS/PFCzIrPiq4+PBD (30 wt%)/TPBI/Ba/Al (PBD: 5-(4-*tert*-butylphenyl)-2-(biphenyl-4-yl)-1,3,4-oxadiazole; TPBI: 1,3,5-tris-(2-*N*-phenylbenzimidazolyl)-benzene). A maximum external quantum efficiency (EQE) of 7.3% and a luminous efficiency (LE) of 6.9 cd A^{-1} with a luminance of 138 cd m^{-2} were achieved at a current density of 1.9 mA cm^{-2}. The efficiencies remained as high as EQE = 3.4% and LE = 3.3 cd A^{-1} with a luminance of 3770 cd m^{-2} at a current density of 115 mA cm^{-2}. The single-layer devices based on charged Ir polymers also showed high efficiency with the high work-function metal Ag as cathode. The maximum external quantum efficiencies of the devices were 0.64% and 0.66% for PFPIrPiq2 and PFPIrPiq10, respectively. A possible mechanism of an electrochemical cell associated with its electrochemical redox pathway for single-layer devices has been proposed. The results showed that the charged Ir polymers are promising candidate materials for polymer optoelectronic devices.

Keywords: host–guest systems · iridium · luminescence · N ligands · polymers

Introduction

Electrophosphorescent polymers containing transition metal complexes have attracted much attention since researchers realized their potential practical applications in the preparation of high-efficiency polymer light-emitting diodes (PLEDs).[1] Strong spin–orbit coupling of transition metal ions in complexes can provide relatively short lifetimes of triplet metal-to-ligand charge-transfer (^{3}MLCT) states, thereby theoretically achieving nearly 100% internal quantum efficiency.[2] The chemistry and photophysics of polymers containing ruthenium bipyridyl and terpyridyl complexes in their main chains and side chains have been studied extensively,[3] while many reports have recently focused on different types of electrophosphorescent polymers based on neutral iridium complexes for optoelectronic applications, due to their relatively short phosphorescent lifetimes and high luminous efficiencies. Nonconjugated polymers with attached neutral iridium complex pendants have been reported by Lee and Tokito.[4] High external quantum efficiencies based on those polymers were achieved in red, green, and blue PLEDs. Phosphorescent conjugated polymers based on polyfluorene backbones with neutral iridium complex pendants attached to the 9-carbon position of fluorene were reported by Chen,[5] and well defined main-chain-type oligo- and polyfluorenyl biscyclometalated iridium complexes were reported by Sandee.[6] Fluorene-*alt*-carbazole copolymers with 1-phenylisoquinoline–Ir complexes grafted in the carbazole N-position and chelating copolymers based on iridium complexes in the main chain can achieve high external quantum efficiencies in PLEDs.[7,8]

Neutral iridium complexes have attracted much more interest than ionic iridium complexes, probably due to their

[a] B. Du, L. Wang, Dr. H. Wu, Prof. W. Yang, Y. Zhang, R. Liu, M. Sun, Prof. J. Peng, Prof. Y. Cao
Institute of Polymer Optoelectronic Materials and Devices
Key Lab of Special Functional Materials, Ministry of Education
South China University of Technology, Guangzhou, 510640 (China)
Fax: (+86) 20-8711-0606
E-mail: pswyang@scut.edu.cn
psjbpeng@scut.edu.cn

compatibility with hydrophobic matrices and their lack of counterions, which can result in time delays between the switch-on and the observed emission in display-related applications. However, charged iridium complexes also show excellent electrochemical, photochemical, and thermal stability, good charge-transport properties, long-lived excited states, and good photoluminescence (PL) efficiencies.[9] They have been regarded as promising candidates for application in solid-state electroluminescent devices, due to the presence in them of a single, solution-processable layer sandwiched with high efficiency between two air-stable electrodes. Recently, light-emitting diodes (LEDs) and solid light-emitting electrochemical cells (LECs) based on charged iridium complexes have shown some distinct advantages over electroluminescent devices based on neutral iridium complexes.[10]

Charged iridium complexes of low molecular weight are doped into a polymeric matrix for the polymer light-emitting diode fabrication process, and these devices are found to be significantly less efficient than those with neutral complexes.[10] The difference in efficiency is probably attributable to the ionic content and the charge-trapping properties of charged iridium complexes. Recently, Brunner et al.[10b] have reported that the low efficiencies and high switch-on voltages of charged-complex-based devices could be overcome by utilizing a hole-blocking layer to modify the charge injection and charge transport.

Although devices from phosphorescent dyes doped into polymeric host materials showed high efficiency in polymer light-emitting diodes,[1g,7b] device performance from blend systems is always limited by phase separation and aggregation of dopants. This problem is even more serious for charged complexes doped into a neutral wide-band-gap polymer host, since polar charged iridium complexes have poorer compatibility with typical hydrophobic host polymers. Therefore, a polymeric host incorporating covalently bonded phosphorescent chromophores has been regarded as an efficient solution with the additional benefits of excellent solution processability and stability.[5–8] Charged Ir complex molecules covalently attached to polymer main chains or side chains would be forced to separate from each other and so should be more homogeneously dispersed into the polymer matrix.[12] The performances of PLEDs based on copolymers containing Ir complexes can be further improved by the choice of a suitably charged iridium complex, the match of the iridium complex with the host backbone, and optimization of the device structure.

The study of polymeric materials functionalized with coordinating charged iridium moieties is currently a rapidly expanding field in macromolecular chemistry. Solution-processable monoterpyridine–PEG-functionalized charged iridium(III) complexes and phosphorescent side-chain functionalized poly(norbornene)s containing charged iridium complexes as light-emitting polymeric materials have been successfully synthesized,[11] but these novel nonconjugated polymers do not have the advantages of conjugated polymers, such as fluent charge transportability. Recently, polyfluorenes containing charged iridium complexes in their backbones have received a great deal of attention. Soluble π-conjugated polymers with charged iridium complexes in their backbones have been synthesized.[12] The polymers showed efficient energy transfer and good redox reversibility and film formation.

Although a considerable number of studies have focused on charged Ir polymers, π-conjugated polymers with charged iridium complexes in their side chains had not previously been reported, while even less was known about the photophysical properties of those polymers in the preparation of optoelectronic devices. In the work reported here, polymers with charged iridium complexes in their side chains were successfully synthesized. 2-(Pyridin-2-yl)benzimidazole and 1-phenylisoquinoline were selected as ligands because the obtained metal complexes often show attractive chemical and physical properties.[13,14] Their synthesis and characterization are described, together with detailed studies of the electroluminescent properties.

Results and Discussion

Synthesis and structural characterization: The synthetic routes to the macroligands (PFCz and PFP) are shown in Scheme 1. 3,6-Dibromo-9-{*N*-[2-(pyridin-2-yl)benzimidazole]hexyl)carbazole was synthesized through a coupling reaction between 2-(pyridin-2-yl)benzimidazole and 3,6-dibromo-9-(6-bromohexyl)carbazole in the presence of sodium hydroxide by the published procedure.[15]

The macroligands were synthesized by Suzuki polycondensation. The feed ratios of monomer (**4** or **5**) to **6** were 50:50 and the corresponding macroligands were named PFCz and PFP, respectively. All the macroligands readily dissolve in common organic solvents such as chloroform, THF, toluene, and xylene. The number-average molecule weights (M_n) of PFCz and PFP are 23305 and 6987, respectively, with polydispersity indexes (PDIs) of 1.63 and 1.74.

The synthetic routes to the model charged iridium complex Ir(1-piq)$_2${*N*-[2-(pyridin-2-yl)benzimidazole]-hexyl}$^+$ BF_4^- (IrPiq) and the corresponding charged Ir polymers are depicted in Scheme 2. The polymers containing charged iridium complexes of different composition in their side chains were directly prepared by heating the chloride-bridged iridium dimer and the macroligand PFP at reflux solvent in the presence of $NaBF_4^-$. The resulting solution was concentrated, and the concentrate was dropped into methanol to precipitate the polymer. After precipitation, all polymers were washed with methanol at reflux in a Soxhlet extractor for 2 d, in order to remove the chloride-bridged iridium dimers and $NaBF_4^-$ in polymers; the corresponding polymers were named PFPIrPiq2, PFPIrPiq4, and PFPIrPiq10, respectively. The charged iridium complex contents in the polymers were estimated by X-ray fluorescence spectrometry (XRF), and the results indicated that the actual iridium complex contents in the polymers were lower than the feed ratios (Table 1). The weak ^{1}H NMR signal of the H atom in the

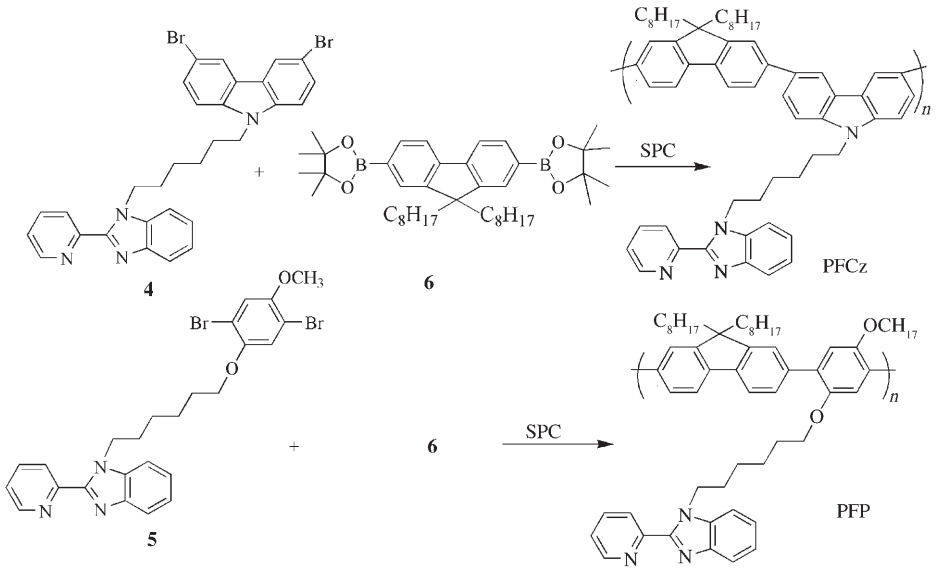

Scheme 1. Synthetic routes to macroligands.

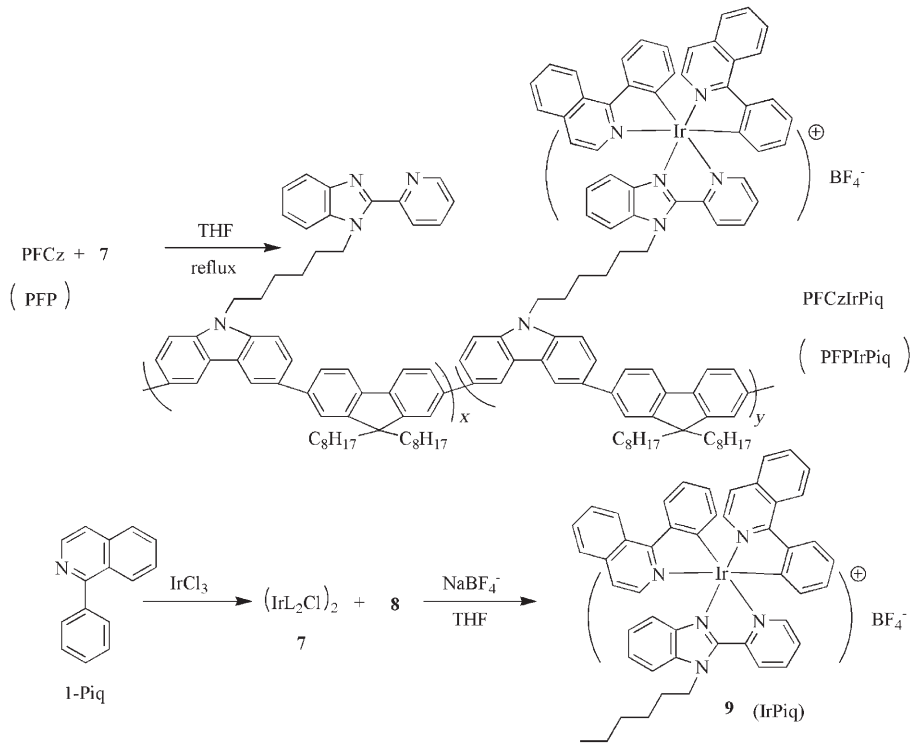

Scheme 2. Synthetic routes to charged Ir polymers.

IrPiq unit is observable in the charged copolymers with high contents of Ir complex (PFCzIrPiq10 or PFPIrPiq10).

Optical and electrochemical properties: The absorption spectrum of the charged iridium complex (IrPiq) in film is shown in Figure 1. There are broad bands from 270 to 500 nm, the most intense at $\lambda < 300$ nm, and moderately intense bands at longer wavelengths. The absorption bands ($\lambda < 300$ nm) are mainly due to spin-allowed $^1\pi$–π^* ligand-centered (LC) transitions and the absorption band in the 420–500 nm region might be due to the spin-allowed singlet metal-to-ligand charge-transfer (^{1}MLCT) transitions[20] and spin-forbidden triplet metal-to-ligand charge transfer (^{3}MLCT) transitions of the iridium complex.[21] There is good overlap between the absorption of the guest IrPiq and the PL spectra of the host macroligands (PFCz and PFP), as shown in Figure 1, so efficient Förster energy transfer from the singlet excited state of the host to the ^{1}MLCT band of the iridium complex can be expected.[7]

In Figure 2, the absorption spectra of the charged Ir polymers show no essential differences from those of their host macroligands, obviously as a result of the low Ir complex content in the polymers. The absorption of the polymers (PFCzIrPiq10) was red-shifted by only 2 nm in relation to that of the host macroligand (PFCz). The absorption peaks at 346 and 371 nm can be attributed to the π–π^* transitions of PFCz and PFP backbones, respectively, while the peak at 317 nm is due to the pendant 2-(pyridin-2-yl)benzimidazole group in comparison with the absorption of 2-[*N*-(pyridin-2-yl)hexyl]benzimidazole. The blue shift ($\Delta\lambda = 30$ nm) of the absorption peak of PFCz in relation to the PFP backbone implies that the conjugation length of the PFCz

Table 1. Compositions of copolymers containing iridium complexes.

Polymer	Ir complex content [mol %] in feed ratio[a]	Ir complex content [mol %] in polymer[b]
PFPIrPiq2	2	1.5
PFPIrPiq4	4	2.7
PFPIrPiq10	10	9.0
PFCzIrPiq4	4	2.56
PFCzIrPiq10	10	10.7

[a] Chloride-bridged Ir-dimer/repeated unit of macroligand. [b] IrPiq/repeated unit of macroligand.

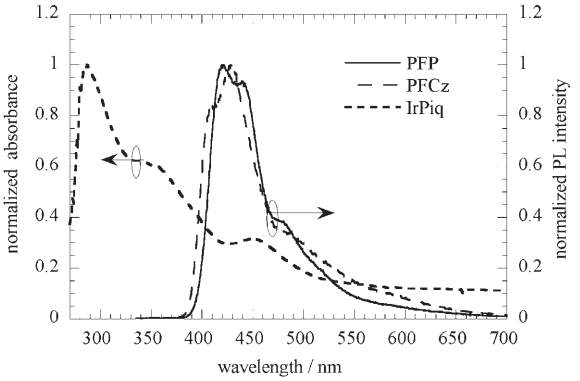

Figure 1. UV/Vis absorption spectrum of IrPiq and PL spectra of macroligands in films.

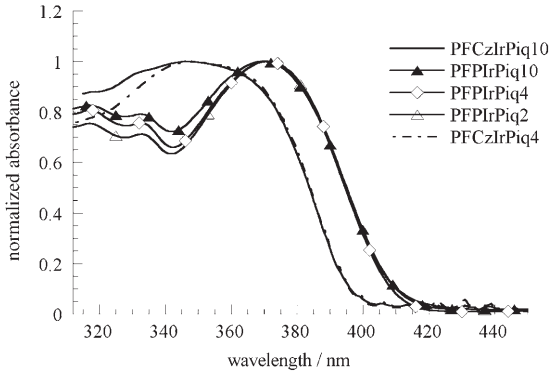

Figure 2. UV/Vis absorption spectra of charged Ir polymers in film.

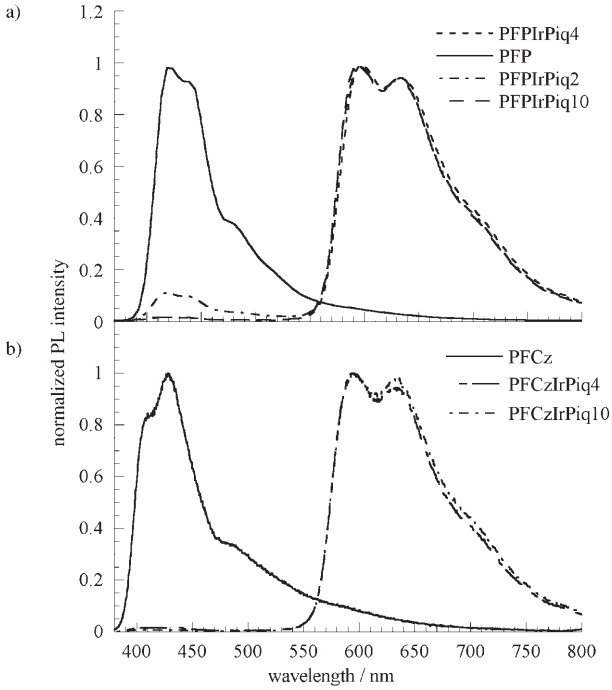

Figure 3. PL spectra of charged Ir polymer a) PFPIrPiq and b) PFCzIrPiq in films.

backbone effectively decreases, as the linear π-system is interrupted by the carbazole unit at the 3,6-linkage.[22]

The photoluminescence (PL) spectra of the charged polymers are shown in Figure 3. The maximum emission peak of the charged polymers is at 595 nm, the same as the PL emission of the IrPiq complex doped in the macroligand PFP (Figure 4). In Figure 3, the emission peak at 420 nm can be observed for the PFP-based copolymers with low Ir complex content of 2 mol% (actual Ir content: 1.5 mol%). This implies that the energy transfer from the main chain to the Ir complex attached at the alkyl side chain of the PFP is incomplete, probably because the average distance from a photoexcited polymer chain to the nearest Ir complex is too long.[7] The emissions both from the PFCz and from the PFP backbone are completely quenched for copolymers with Ir complex contents of 4 mol%, which indicates that the energy transfer becomes complete with increasing Ir complex content in the copolymers. The charged Ir polymers show high PL efficiencies (in Table 2), relative to IrPiq complex ($Q_{PL}\% = 5.4\%$) because the concentration quenching and T–T annihilation are greatly decreased. It is also shown that the incorporation of a space between the polymer host and phosphorescent guest might be a good design principle for achieving electrophosphorescent polymers with higher PL efficiencies.[7d] Figure 4 shows the PL spectra for the blends of IrPiq doped in host PFP. The IrPiq contents in PFP were 2, 4, and 10 mol%, respectively (actual Ir contents: 1.5, 2.7 and 9 mol%), in relation to the corresponding charged iridium copolymers of the same composition. In contrast with the copolymer with the charged Ir complex incorporated into the side chain, in which host emission was almost completely quenched for PFPIrPiq4 (Figure 3), the blend with 10 mol% complex shows incomplete quenching with a moderate host emission peaking at 420 nm. This shows that much more efficient energy transfer occurs in the charged iridium copolymers than in the blend system. This

Table 2. Optical and electrochemical properties of macroligands and charged Ir polymers.

Polymer	$\lambda_{max\ (Abs)}$ [nm]	$\lambda_{max\ (PL)}$ [nm]	PL [%]	E_g^{opt} [eV]	E_{ox} [V]	HOMO [eV]	LUMO[a] [eV]
PFCz	346	428	30	3.12	0.95	−5.35	−2.23
PFP	317, 371	420	43	3.01	1.28	−5.68	−2.67
PFCzIrPiq4	346	595	43	3.09	0.98	−5.38	−2.29
PFCzIrPiq10	348	595	41	3.10	0.95	−5.35	−2.25
PFPIrPiq2	317, 371	595	42	3.03	1.29	−5.69	−2.66
PFPIrPiq4	317, 371	595	54	3.03	1.31	−5.71	−2.68
PFPIrPiq10	317, 371	595	34	3.03	1.30	−5.70	−2.67

[a] Calculated from HOMO level and the optical band gap.

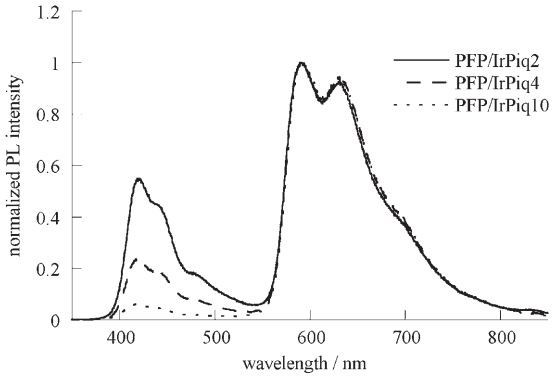

Figure 4. PL spectra for PFP/IrPiq blends in films.

in turn indicates a great advantage of incorporation of charged complexes covalently into polymer side chains, because the complexes are distributed more homogeneously in the polymer host, while in the blend system Ir complexes are easily aggregated due to poor compatibility between the hydrophobic conjugated host polymer and polar charged IrPiq complexes.[7,8,12]

The electrochemical characteristics of the macroligand and Ir polymer thin films coated onto Pt electrodes were investigated by cyclic voltammetry (CV). The highest occupied molecular orbital (HOMO) levels were calculated by the empirical formula $E_{HOMO} = -e(E_{ox}+4.4)(eV)$, where E_{ox} is the onset oxidation potential versus a saturated calomel electrode (SCE). As no reversible *n*-doping process was observed in the cyclic voltammograms, the LUMO levels were estimated from the HOMO values and values of optical band gaps (E_g^{opt}) by $E_{LUMO} = E_{HOMO} + E_g^{opt}$. The optical band gap was obtained from $E_g^{opt} = 1240/\lambda_{edge}$, where λ_{edge} is the onset value of the absorption spectrum of the solid film in the long-wavelength direction.[16,23] The electrochemical data for the polymers are summarized in Table 2. The HOMO and LUMO levels of the charged Ir polymers showed no essential differences from those in their corresponding macroligands, which further indicated that the attachment of IrPiq in the side chain did not alter the backbone and conjugation length of the host polymer.[7,23c] Unfortunately, the redox peaks of IrPiq in all Ir polymers proved to be unrecordable, obviously due to the low Ir complex contents in the polymers. For isolated IrPiq, the measurements were carried out at room temperature in argon-saturated acetonitrile solutions containing tetrabutylammonium hexafluorophosphate (Bu_4NPF_6; 0.1 M) with platinum working electrodes at a scan rate of 50 mV s^{-1} and IrPiq concentrations of about 2×10^{-4} M. An oxidation wave at +1.10 V vs. SCE was recorded. The HOMO level of IrPiq is evaluated at −5.5 eV. The LUMO level (−3.2 eV) was obtained from the onset of absorption and HOMO level.[7e] On the assumption of no great changes in the LUMO level of the IrPiq grafted into host polymer chains, the grafted Ir complex will function as an electron trap.

Electrophosphorescent properties: Double-layer devices with the configuration of ITO/PEDOT:PSS (50 nm)/polymers+PBD (30 wt%) (75 nm)/Ba (4 nm)/Al(150 nm) were fabricated. PBD was doped to improve the electron-transporting capability of the polymers.[24a] As can be seen in Figure 5, EL emission from the polymer backbones was

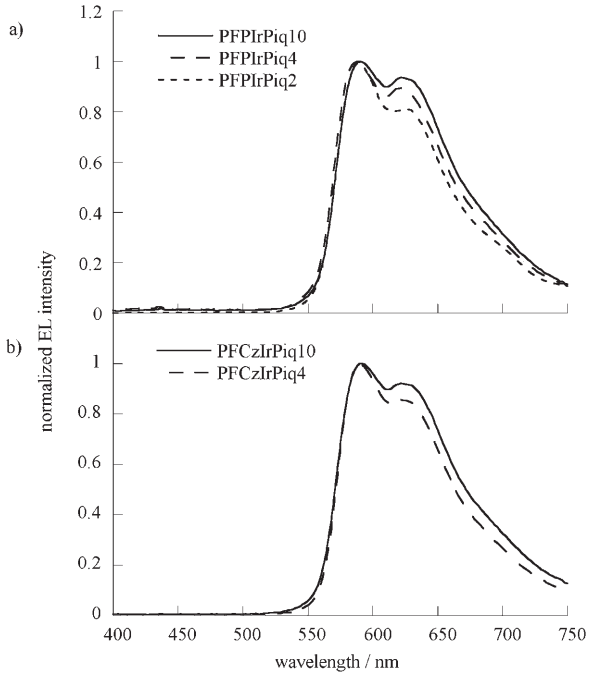

Figure 5. EL spectra of devices fabricated from a) PFPIrPiq and b) PFCzIrPiq.

completely quenched even though the actual IrPiq content of PFPIrPiq2 was as low as 1.5 mol%, which indicates that there is efficient energy transfer from the host to the guest or charge trapping. Similar PL and EL spectra phenomena were observed by Chen when neutral iridium complex pendants were attached to the 9-carbon position of fluorene.[5] Emission peaks at 595 nm were observed for PFCzIrPiq and PFPIrPhq. The emissions from devices are dominated by iridium complex phosphorescent emissions, which are almost identical in peak position and line-width for all polymers. The device performances are shown in Table 3. The devices produced from PFP-based polymers have higher efficiencies than those from PFCz-based polymers. A maximum external quantum efficiency of 1.3% and a luminous efficiency of 1.2 cd A^{-1} were achieved from PFPIrPiq2. For PFCzIrPiq devices, because of the lower hole injection barrier (ca. 0.15 eV; Figure 7b) at the PEDOT:PSS/PFCzIrPiq interface and the good hole transporting capabilities of carbazole-based polymers,[24b,25] the holes are majority carriers unlike the PFPIrPiq devices. On the other hand, from CV measurements, it is clear that the HOMO level of the IrPiq complex is lower than that of PFCz, which means that IrPiq cannot trap holes in PFCzIrPiq polymers. However, for PFPIrPiq devices, the lower HOMO level of PFP makes IrPiq com-

Table 3. Device performances of charged Ir polymers in different configurations.

Polymer	Turn-on [V]	EQE_{max} [%]	LE_{max} [cd A^{-1}]	L_{max} [cd m^{-2}]	$J = 30$ mA cm^{-2}			
					Bias [V]	L [cd m^{-2}]	LE [cd A^{-1}]	EQE [%]
PFPIrPiq2[a]	11	1.3	1.2	262	17	251	0.8	0.8
PFPIrPiq4	9.5	1.1	1.0	537	13	297	0.9	1.0
PFPIrPiq10	11	1.0	0.9	461	16	266	0.7	0.9
PFCzIrPiq4	9	0.6	0.5	986	15	140	0.5	0.5
PFCzIrPiq10	9.5	0.5	0.5	577	14	137	0.4	0.5
PFPIrPiq2[b]	11	4.1	3.9	476	20	467	1.5	1.6
PFPIrPiq4	10	4.7	4.5	1396	17	916	2.7	2.8
PFPIrPiq10	10.5	2.6	2.4	764	19	479	1.5	1.6
PFCzIrPiq4	10	7.3	6.9	4004	20	1452	4.5	4.7
PFCzIrPiq10	9.5	5.7	5.4	3945	17	1380	4.5	4.6

[a] ITO/PEDOT:PSS/polymer+PBD(30 wt %)/Ba/Al. [b] ITO/PEDOT:PSS/polymer+PBD(30 wt %)/TPBI/Ba/Al.

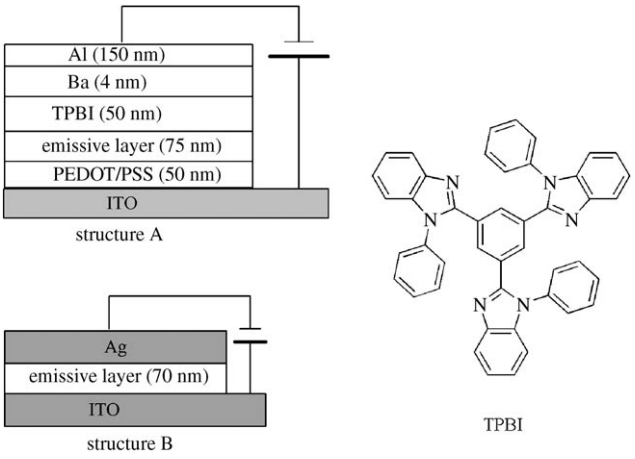

Figure 6. Schematic diagrams of the device configurations and the molecular formula of TPBI.

plex trap the holes in PFPIrPiq polymers. As a result, hole and electron currents are significantly unbalanced in PFCzIrPiq devices, leading to lower device efficiencies than in PFPIrPiq. In order to enhance PFCz-based device performances, it is necessary to achieve hole injection/transport attenuation or electron flux enhancement, which can shift the recombination zone away from the cathode interface.

One method for testing this assumption is by inserting an organic hole-blocking and electron-transporting layer between the emissive layer and the cathode. A suitable material for such a layer is TPBI, which can be vacuum-evaporated on top of the polymer layer prior to vacuum evaporation at the cathode. TPBI has a very low-lying HOMO level at −6.2 eV (hence its hole-blocking capabilities) and a large HOMO–LUMO energy difference of 3.4 eV (hence its exciton-blocking capabilities). Multi-layer devices with the configuration of ITO/PEDOT:PSS (50 nm)/polymers+PBD (30 wt %) (75 nm)/TPBI (50 nm)/Ba (4 nm)/Al (150 nm) (structure A, as shown in Figure 6) were fabricated. The HOMO energy level of TPBI is 0.85 eV higher than that of PFCz, which produces a high hole barrier and obstructs the hole transport. The *J–V* curves and energy diagrams of device components provide further insight into the roles played by the functional material TPBI in the device (Figure 7). As shown in Figure 7 and Table 3, the current-voltage characteristic is shifted to higher voltage and the device performances are obviously enhanced after insertion of a TPBI layer. Similar *J-V* characteristics can be observed for the devices produced from other Ir polymers (not shown here). Preliminary device performances are summarized in Table 4. The best device performances were obtained from PFCzIrPiq4. A maximum external quantum efficiency of 7.3% and a luminous efficiency of 6.9 cd A^{-1} with a luminance of 138 cd m^{-2} were achieved at a current density of 1.9 mA cm^{-2}. The efficiencies of this device remained as high as EQE = 3.4% and LE = 3.3 cd A^{-1} with a luminance of 3770 cd m^{-2} at a current density of 115 mA cm^{-2}. The PFCzIrPhq10 device showed EQE = 5.7% and LE = 5.4 cd A^{-1} with a luminance of 321 cd m^{-2} at a current density of 5.9 mA cm^{-2}. At a current density of 100 mA cm^{-2}, the efficiencies of this device re-

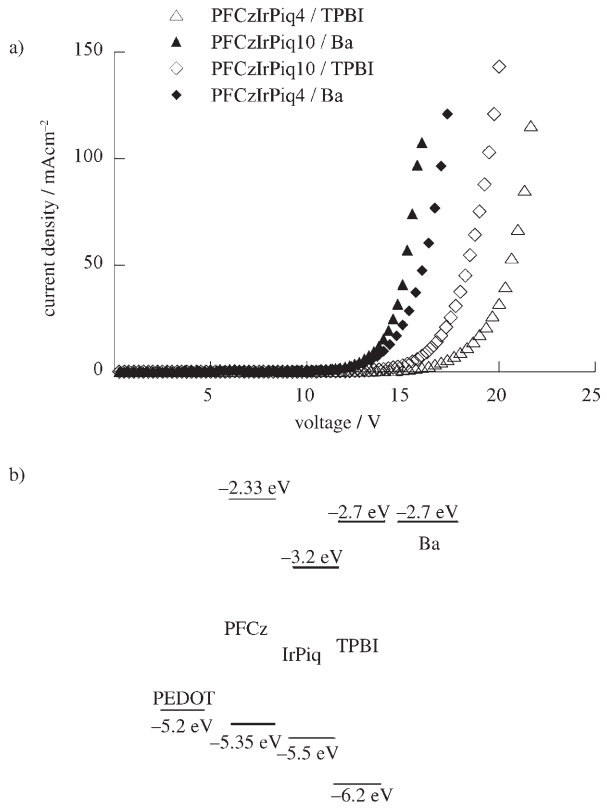

Figure 7. *J-V* curves of devices based on a) PFCzIrPiq and b) energy diagram of the device components.

Table 4. Device performances with different cathodes.

Polymer	Turn-on [V]	EQE_{max} [%]	L_{max} [cd m^{-2}]	$J = 35$ mA cm^{-2}			
				Bias [V]	L [cd m^{-2}]	LE [cd A^{-1}]	EQE [%]
PFPIrPiq2[a]	14	0.83	150	19.5	87	0.25	0.5
PFPIrPiq10	13	0.33	96	17.6	45	0.13	0.3
PFPIrPiq2[b]	11	0.64	200	17.5	86	0.22	0.5
PFPIrPiq10	11	0.66	176	16	67	0.19	0.4

[a] ITO/PEDOT:PSS/polymer/Ba/Al.[b] ITO/polymer/Ag.

mained EQE = 3.4% and LE = 3.2 cd A^{-1} with a luminance of 3330 cd m^{-2}. The luminance (L) and the external quantum efficiency (EQE) of the devices as a function of current density (J) for PFPIrPiq and PFCzIrPiq are shown in Figure 8.

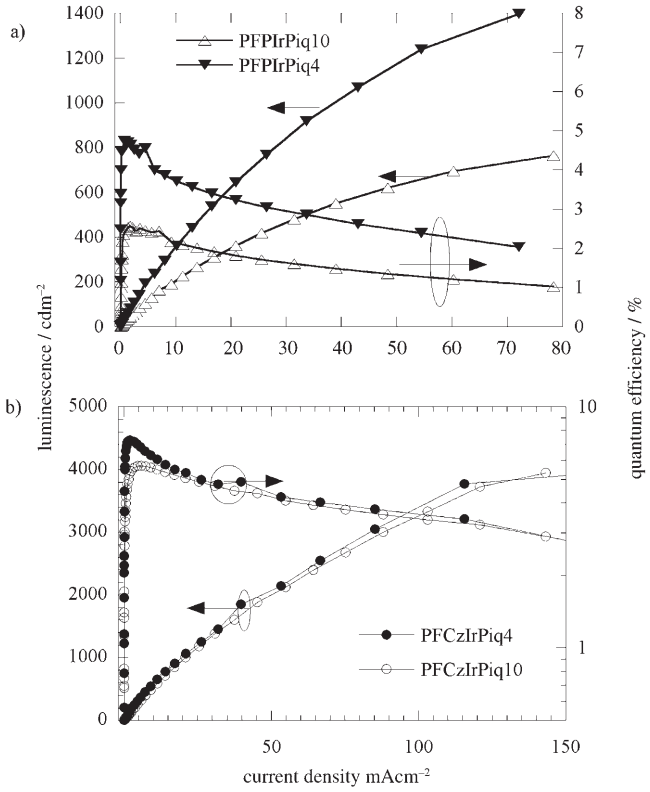

Figure 8. *L–J–QE* curves of the devices fabricated from a) PFPIrPiq and b) PFCzIrPiq.

The device performances of the carbazole-based PFCzIrPiq are obviously superior to those of the benzene-based PFPIrPiq. When a hole-blocking TPBI layer was deposited on the top of active layer, the situation was reversed, which is probably due to significantly reduced hole current in the PFCzPiq-based devices, as the HOMO level of TPBI (−6.2 eV) is much lower than that of PFCzIrPiq (−5.35 eV). As a result of a more balanced hole and electron current, the efficiencies of PFCzIrPiq devices with a TPBI layer are significantly increased. For PFPIrPiq devices, in contrast, because of the smaller difference between the HOMO levels of PFP and TPBI (−5.68 eV vs −6.2 eV), TPBI is a less efficient hole blocker for the PFPIrPiq device. The increases in efficiencies of all devices are due to the reductions of both hole current and metal cathode quenching. A reservoir of holes builds up within the layer close to the TPBI layer and the holes are shielded from annihilation at the cathode by the TPBI layer.

Although high luminous efficiency was obtained at small current densities (typically less than 10 mA cm^{-2}), the maxima of luminance of all the devices based on the polymers with charged iridium complexes in their side chains were lower than those of some previously reported PLEDs with doped neutral phosphorescent red or red-orange iridium complexes as emitters. As shown in Table 3 and Figure 8b, maximum luminances of 4004 cd m^{-2} for PFCzIrPiq4 and 3945 cd m^{-2} for PFCzIrPiq10 devices were observed at the current density of around 150 mA cm^{-2} when TPBI was employed as hole-blocking layer. The devices showed relatively higher EL brightness in relation to devices produced from the red phosphorescent conjugated polymers[26a] containing charged iridium complexes in the backbones, probably owing to the high PL efficiencies.

The efficiencies of the devices decayed at a high rate with varying current density or operating voltage, as shown in Figure 8. A similar phenomenon has been reported in devices based on charged iridium, ruthenium, and osmium complexes. A voltage above the redox potential of the charged transition metal complexes can lead to the fast degradation of devices. Bard's group[26b] reported that degradation of devices containing charged $[Ru(bpy)_3]^{2+}$ originated from a reaction with water and the subsequent production of $[Ru(bpy)_2(H_2O)_2]^{2+}$, leading to EL quenching. The reasons for the degradation in the charged iridium complex-based devices are not completely understood at present. A similar mechanism might be at work in our charged Ir polymers.

Another possible mechanism leading to low EL luminance in the devices might arise from multi-particle annihilation processes, such as triplet-triplet annihilation (TTA),[26c] triplet-polaron quenching,[26d] and field-assisted dissociation of excitons at high electric fields.[26e] These degradations in high current density regions can be remedied by reducing long radiative lifetimes of triplet excited states by chemical modifications. Materials modification is ongoing and improvement should be expected.

EL spectra of the devices produced from IrPiq doped into a PFP host are shown in Figure 9. Comparison of the EL spectra of the devices produced from corresponding charged copolymers (Figure 5) with those of the blends reveals that the former show much more efficient energy transfer than the latter. When the doping concentration is 4 mol%, the host emission is not completely quenched, while the host emission of the charged copolymer containing 2 mol% IrPiq

is quenched completely (Figure 5). This further indicates the advantage of a covalently connected charged phosphorescent dye in a conjugated polymer side chain. This result is consistent with that reported in chelating polymers with neutral Ir complexes in their conjugated backbones.[8]

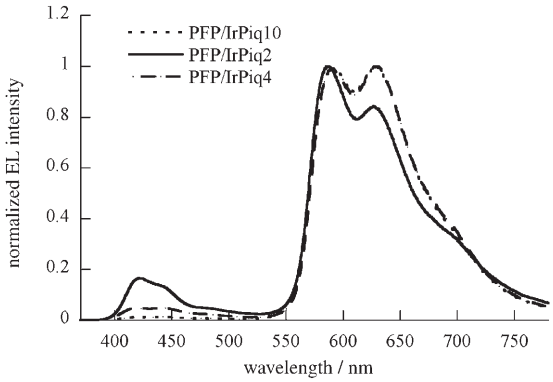

Figure 9. EL spectra of the devices fabricated from PFP/IrPiq blends. Device structure: ITO/PEDOT:PSS (50 nm)/(PFP/IrPiq)+PBD (30 wt %) (75 nm)/TPBI (50 nm)/Ba (4 nm)/Al (150 nm).

Despite the enhanced device performance, as shown in Table 3, the turn-on and operating voltages for all devices based on the resulting polymers are very high. This could be attributable to a charge-trapping mechanism, energetically favored, as inferred from the energy level. To remedy this problem, reducing the content of iridium complex, utilizing proper heat annealing treatment to relieve space charge build-up, and selection of a good electron injection-cathode could be good choices.[27] These efforts are in progress and will be reported in a forthcoming paper.

The single-layer light-emitting devices based on PFPIrPiq2 and PFPIrPiq10 were fabricated with the configuration of ITO/polymer/Ag (structure B, as shown in Figure 6). Large hole and electron injection barriers between the polymer and the electrodes are expected. The device performances at around 35 mA cm^{-2} with Ba/Al and Ag as cathodes are summarized in Table 4. For the single-layer device based on PFPIrPiq2, a quantum efficiency of 0.5 % and a luminous efficiency of 0.22 cd A^{-1} with 86 cd m^{-2} were reached at the current density of 35 mA cm^{-2}, the same as those of the Ba/Al device. Similar results were obtained with PFPIrPiq10. The maximum external quantum efficiencies (EQE_{max}) of the single-layer devices were 0.64 % and 0.66 % from PFPIrPiq2 and PFPIrPiq10, respectively, while EQE_{max} of the double-layer devices with Ba as cathode were 0.83 and 0.33 %, respectively. The maximum luminance of the single-layer device was approximately 200 cd m^{-2}, whereas that of the double-layer device was only 150 cd m^{-2}. Figure 10 compares *J–V* for PFPIrPiq devices with Ba or Ag as cathode. The results clearly indicate that the electron and hole injections from ITO/polymer/Ag device are comparable to those from a low work function Ba cathode with a slight decrease of the operating voltage.

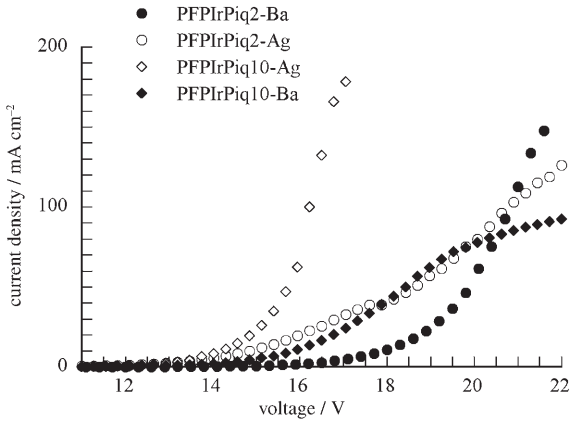

Figure 10. *J–V* curves of PFPIrPiq devices with Ag or Ba/Al cathodes.

There are many functions in which charged iridium complexes could significantly improve electron and hole injection in devices associated with an electrochemical cell mechanism.[9–11] In the emitting layer, we speculated that the introduction of charged IrPiq into the polymer made electrochemical doping at the interface of the film/electrode possible[28] or the formation of an ionic space charge layer easy,[29] which lowered the barrier to hole and electron injection.

Conclusion

High-efficiency electrophosphorescent copolymers containing charged iridium complexes—with a 2-(pyridin-2-yl)benzimidazole moiety in the polymer side chain directly coordinating with a chloride-bridged iridium dimer of 1-phenylisoquinoline—were synthesized. A maximum external quantum efficiency of 7.3 % and a luminous efficiency of 6.9 cd A^{-1} with a luminance of 138 cd m^{-2} were achieved from PFCzIrPiq4 at a current density of 1.9 mA cm^{-2}. The efficiencies of this device remained as high as EQE = 3.4 % and LE = 3.3 cd A^{-1} with a luminance of 3770 cd m^{-2} at a current density of 115 mA cm^{-2}. The enhancement of the device performances could be attributed to the balanced charge injection and transport achieved through insertion of a layer of TPBI. The maximum external quantum efficiencies of single-layer devices were 0.64 % and 0.66 % for PFPIrPiq2 and PFPIrPiq10, respectively, with Ag as cathode. The encouraging results obtained with the devices indicate that the copolymers containing charged iridium complexes are promising in optoelectronic applications.

Experimental Section

Measurements: ^{1}H and ^{13}C NMR spectra were recorded on a Bruker DRX 300 spectrometer operating at 300 and 75 MHz, respectively, with tetramethylsilane as a reference. EI-MS were recorded on a LCQ DECA XP Liquid Chromatograph/Mass Spectrometer (Thermo Group).

The molecular weight of the polymers was determined with a Waters GPC 2410 instrument in tetrahydrofuran (THF) by use of a calibration curve of polystyrene standards. Elemental analyses were performed on a Vario EL elemental analysis instrument (Elementar Co.). The iridium contents analyses were determined with a Philips (Magix PRO) sequential X-ray fluorescence (XRF) spectrometer, with a rhodium tube operated at 60 kV and 50 mA, a LiF 200 crystal, and a scintillation counter. Iridium(III) 2,4-pentanedionate (from Alfa Aesar Co.) was used as a standard. UV/Vis absorption spectra were recorded on a HP 8453 spectrophotometer. Cyclic voltammetry was carried out on a potentiostat/galvanostat model 283 (Princeton Applied Research) with a platinum electrode at a scan rate of 50 $mV\,s^{-1}$ against a saturated calomel electrode (SCE) with a nitrogen-saturated solution of tetrabutylammonium hexafluorophosphate (Bu_4NPF_6, 0.1 M) in acetonitrile (CH_3CN). Absolute PL efficiencies were measured in an integrating sphere (IS-080, Labsphere) under the 325 nm line of a HeCd laser. Photoluminescence (PL) spectra was recorded with a CCD spectrophotometer (Instaspec 4, Oriel) with 325 nm excitation by a HeCd laser.

Materials: Reactions involving air-sensitive reagents were performed under dry argon. All reagents, unless otherwise specified, were obtained from Aldrich, Acros, and TCI Co, and were used as received. 1-Phenylisoquinoline (1-piq) was prepared by the published procedure.[17]

3,6-Dibromo-9-(6′-bromohexyl)carbazole (1): 3,6-Dibromocarbazole (10 g, 30.8 mmol) in dry THF (50 mL) was added dropwise to a solution of sodium hydride (2.47 g, 61.6 mmol, 60%) in dry THF (50 mL). The mixture was heated at reflux under N_2 for 1.5 h, and the resulting mixture was then added dropwise to 1,6-dibromohexane (90 mmol) in THF (10 mL). The reaction mixture was heated at reflux for another 24 h and was then allowed to cool to room temperature. It was extracted with dichloromethane, followed by washing with water. The oil phase was separated and dried overnight with $MgSO_4$. The solvent was removed by evaporation, and the crude product was purified by silica column chromatography to give a white solid (9.1 g, 60%). ^{1}H NMR (300 MHz, $CDCl_3$): $\delta = 8.14$ (d, $J = 1.8$ Hz, 2H; Cz-H), 7.52 (m, 2H), 7.20 (t, $J_1 = 6.1$ Hz, $J_2 = 2.5$ Hz, 2H; Cz-H), 4.23–4.21 (t, $J_1 = 6.9$ Hz, $J_2 = 7.2$ Hz, 2H; Cz N-CH_2), 3.33–3.30 (m, 2H; Br-CH_2), 1.85–1.81 ppm (m, 8H; CH_2) (aliphatic); ^{13}C NMR (75 MHz, $CDCl_3$): $\delta = 139.28$, 129.07, 123.49, 123.30, 112.05, 110.32 (carbazole ring), 43.13 (N-CH_2), 33.56, 32.46, 28.68, 27.81, 26.36 ppm; elemental analysis (%) calcd for $C_{18}H_{18}NBr_3$: C 44.26, H 3.70, N 2.86; found: C 44.75, H 3.83, N 2.85.

1,4-Dibromo-2-methoxy-5-[(6′-bromo)hexyloxy]benzene (2): A solution of bromine (0.64 g, 4.1 mmol) in chloroform (50 mL) was slowly added at 0°C to a solution of 1-(6-bromohexyloxy)-4-methoxybenzene (5.6 g, 20 mmol) in chloroform (100 mL). The mixture was stirred at room temperature for 24 h and the mixture was neutralized with iced aqueous KOH. After washing with water, diluted hydrochloride acid solution, and brine, the organic layer was dried over $MgSO_4$. Removal of the solvent, followed by recrystallization from ethanol, afforded a white solid (6.5 g, 75%). ^{1}H NMR (300 MHz, $CDCl_3$): $\delta = 7.11$ (s, 2H; Ar-H), 4.01–3.96 (t, $J = 6.4$ Hz, 2H; OCH_2), 3.87 (s, 3H; OCH_3), 3.47–3.43 (t, $J = 7.1$ Hz, 2H; Br-CH_2), 1.93–1.54 ppm (m, 8H; CH_2) (aliphatic); ^{13}C NMR (75 MHz, $CDCl_3$): $\delta = 150.57$, 150.05, 118.67, 117.01, 111.28, 110.42, 70.08, 57.01, 33.77, 32.66, 28.94, 27.83, 25.21 ppm; elemental analysis (%) calcd for $C_{13}H_{17}O_2Br_3$: C 35.10, H 3.82; found: C 35.13, H 4.06.

2-(Pyridin-2-yl)benzimidazole (3):[14] Picolinic acid (40.0 mmol, 4.92 g) and *o*-phenylenediamine (40.0 mmol, 4.32 g) were added to polyphosphoric acid (85%, 100 mL), and the mixture was then heated to 190°C. After 8 h, the solution was cooled and added to ice water (1000 mL). The solution was made alkaline (pH 10, NaOH) and allowed to stir overnight, forming a purple/lavender precipitate, which was filtered and collected. Further purification to remove any excess o-phenylenediamine was achieved by reprecipitation. The lavender precipitate was dissolved in sodium carbonate solution (10%, 200 mL) and stirred to dissolve all of the material. The pH of the solution was brought from 11 to 7.8, resulting in the reprecipitation of the lavender product. The precipitate was collected by filtration, dried, and weighed. The product was further purified by column chromatography and recrystallization to give a white solid (1.95 g, 25%). ^{1}H NMR (300 MHz, $CDCl_3$): $\delta = 8.54$ (d, $J = 4.8$ Hz, 1H; Py-H), 8.49 (t, $J = 7.9$ Hz, 1H; Py-H), 7.92–7.87 (m, 2H; Py-H), 7.39–7.26 ppm (m, 4H; Ar-H).

3,6-Dibromo-9-{*N*-[2-(pyridin-2-yl)benzimidazole]-hexyl}carbazole (4):[15] A mixture of 3,6-dibromo-9-(6′-bromohexyl)carbazole (4.88 g, 10 mmol), 2-(pyridin-2-yl)benzimidazole (1.95 g, 10 mmol), sodium hydroxide (0.44 g, 11 mmol), and dimethyl sulfoxide (30 mL) was stirred and heated at 130°C for 24 h under argon. It was subsequently poured into ice water (100 mL). After extraction with CH_2Cl_2 (3×30 mL), the organic layer was washed with water and dried over anhydrous $MgSO_4$, and the solvent was then evaporated. The resulting residue was purified by silica gel column chromatography (petroleum ether/ethyl acetate 2:1) to give a white solid product (2.7 g, 43%). ^{1}H NMR (300 MHz, $CDCl_3$): $\delta = 8.54$–8.52 (d, $J = 4.8$ Hz, 1H; Py-H), 8.43–8.40 (d, $J = 7.9$ Hz, 1H; Py-H), 8.15–8.14 (d, $J = 1.8$ Hz, 2H; Cz-H), 7.87–7.81 (m, 2H; Py-H), 7.54–7.51 (dd, $J = 1.9$ Hz, 2H; Cz-H), 7.39–7.28 (m, 4H; Ar-H), 7.22–7.19 (m, 2H; Cz-H), 4.80 (t, $J = 7.3$ Hz, 2H; benzimidazole N-CH_2), 4.20 (t, $J = 7.0$ Hz, 2H; Cz N-CH_2), 1.88–1.33 ppm (m, 8H; CH_2) (aliphatic); ^{13}C NMR (75 MHz, $CDCl_3$): $\delta = 150.63$, 149.74, 148.51, 142.58, 139.24, 136.80, 136.54, 129.05, 124.67, 123.74, 123.73, 123.50, 122.60, 120.15, 112.02, 110.30, 110.09, 45.20 (Bm N-CH_2), 43.12 (Cz N-CH_2), 29.85, 28.72, 26.80, 26.53 ppm (aliphatic); elemental analysis (%) calcd for $C_{30}H_{26}N_4Br_2$: C 59.80, H 4.32, N 9.30; found: C 59.89, H 4.50, N 9.30.

1,4-Dibromo-2-methoxy-5-{*N*-[2-(pyridin-2-yl)benzimidazole]-hexyloxy}-benzene (5): This compound was prepared by the same procedure as used to make **4** (yield 65%). ^{1}H NMR (300 MHz, $CDCl_3$): $\delta = 8.71$–8.69 (d, $J = 4.7$ Hz, 1H; Py-H), 8.44–8.41 (d, $J = 8.0$ Hz, 1H; Py-H), 7.84–7.81 (m, 2H; Py-H), 7.44–7.29 (m, $J = 6.8$ Hz, 4H; Ar-H), 7.10–7.07 (d, $J = 5.8$ Hz, 2H; Ar-H), 4.89–4.84 (t, $J = 7.4$ Hz, 2H; benzimidazole N-CH_2), 3.90–3.87 (t, $J = 6.3$ Hz, 2H; OCH_2), 3.82 (s, 3H; OCH_3), 1.94–1.20 ppm (m, 10H; CH_2); ^{13}C NMR (75 MHz, $CDCl_3$): $\delta = 150.73$, 150.54, 150.06, 149.85, 148.66, 142.63, 136.79, 136.63, 124.71, 123.73, 123.27, 122.55, 120.11, 118.66, 117.01, 111.27, 110.46, 110.20, 70.11, 57.01, 45.32, 29.94, 28.93, 26.60, 25.65 ppm; elemental analysis (%) calcd for $C_{25}H_{25}N_3O_2Br_2$: C 53.67, H, 4.48, N 7.51; found: C 53.64, H 4.51, N 7.35.

2,7-Bis(4,4,5,5-tetramethyl-1,3,2-dioxaborolan-2-yl)-9,9-dioctylfluorene (6): This compound was prepared by the published procedure and the obtained boronic ester was recrystallized from methanol to give a white solid product (yield 50%).[7] ^{1}H NMR (300 MHz, $CDCl_3$): $\delta = 7.81$ (m, 2H), 7.76 (s, 2H), 7.72 (m, 2H) (fluorene ring), 1.97 (m, 4H), 1.37 (s, 24H; CH_3), 1.22–0.98 (m, 20H), 0.81 (t, $J = 6.7$ Hz, 6H), 0.54 ppm (m, 4H) (aliphatic); ^{13}C NMR (75 MHz, $CDCl_3$): $\delta = 150.85$, 144.32, 134.06, 129.27, 121.68, 119.75 (fluorene ring), 84.12, 55.56 (C_9-fluorene ring), 40.49, 32.15, 30.32, 29.60, 25.29, 24.01, 23.03, 14.46 ppm (aliphatic); elemental analysis (%) calcd for $C_{41}H_{64}O_4B_2$: C 76.74, H 10.04; found: C 76.43, H 9.95.

Tetrakis(1-phenylisoquinoline-*N*,C2′) (μ-chlorobridged)diiridium(III) (7): Iridium trichloride hydrate (1.318 g, 3.8 mmol) and 1-phenylisoquinoline (1.915 g, 9.4 mmol) were dissolved in a mixture of 2-ethoxyethanol and water (3:1, 20 mL), and the mixture was then heated at reflux for 24 h under argon. The solution was allowed to cool to room temperature, and the deep red precipitate was collected on a glass filter frit. The precipitate was washed with ethanol and ethyl ether to form a dark red power (2.134 g, 90%), which was used directly for the next step without purification.

2-(Pyridin-2-yl)-*N*-hexylbenzimidazole (8): A mixture of 1-bromohexane (15 mmol) and 2-(pyridin-2-yl)benzimidazole (1.95 g, 10 mmol), sodium hydroxide (0.44 g, 11 mmol), and dry dimethyl sulfoxide (30 mL) was stirred and heated at 130°C for 24 h under argon. It was subsequently poured into ice water (100 mL). After extraction with CH_2Cl_2 (3× 30 mL), the organic layer was washed with water and dried over anhydrous Na_2SO_4. The solvent was then evaporated and the obtained residue was purified by silica gel column chromatography (1.12 g, 40%). ^{1}H NMR (300 MHz, $CDCl_3$): $\delta = 8.72$–8.69 (m, 1H, Py-H), 8.44–8.41 (d, $J = 8.0$ Hz, 1H; Py-H), 7.88–7.83 (m, 2H; Py-H), 7.49–7.28 (m, 1H; Ar-H), 7.45–7.28 (m, 3H), 4.87–4.82 (t, $J = 7.6$ Hz, 2H; N-CH_2), 1.92–1.87 (m, 2H), 1.36–1.27 (m, 6H), 0.89–0.85 ppm (m, 3H); ^{13}C NMR (75 MHz, $CDCl_3$): $\delta = 150.68$, 148.63, 136.77, 136.59, 124.73, 123.71, 123.64, 123.23, 122.53, 120.03, 110.25, 45.47, 31.72, 30.40, 26.48, 22.50, 13.98 ppm.

$Ir(1\text{-}piq)_2\{N\text{-}[2\text{-}(2\text{-benzimidazole})pyridine]hexyl\}BF_4^-$ (9):[18] In a round-bottomed flask, dichloro-bridged iridium dimer $[Ir(1\text{-}piq)_2Cl]_2$ (0.10 g, 7.8×10^{-5} mol) and 2-(pyridin-2-yl)-*N*-hexylbenzimidazole (2.0 equiv) were mixed together in THF (25 mL). The solution was then heated at reflux overnight under an inert atmosphere. After the mixture had cooled to room temperature, excess $NaBF_4^-$ in methanol was added dropwise and the mixture was stirred for 4 h, counterion exchange from Cl^- to BF_4^- was performed, the solvent was removed, and the solid was dissolved in CH_2Cl_2 (20 mL). The CH_2Cl_2 solution was filtered off and precipitated in hexane. The product was purified by recrystallization from ethanol (0.1 g, 70%). ^{1}H NMR (300 MHz, $CDCl_3$): $\delta=9.07$–8.89 (m, 2H), 8.75–8.72 (m, 2H), 8.42–8.22 (m, 3H), 7.92–7.71 (m, 7H), 7.61–7.54 (m, 2H), 7.44–7.31 (m, 5H), 7.19–7.11 (m, 2H), 7.01–6.88 (m, 3H), 6.46–6.44 (m, 1H), 6.32–6.29 (m, 1H), 6.04–6.01 (m, 1H), 5.01- 4.88 (m, 3H), 2.10–0.89 ppm (m, 11H); ^{13}C NMR (75 MHz, $CDCl_3$): $\delta=154.72$, 151.83, 151.54, 150.86, 146.83, 146.23, 145.75, 140.90, 140.63, 140.54, 139.23, 136.85, 136.87, 136.56, 133.03, 132.16, 131.62, 131.36, 130.86, 130.71, 130.40, 129.92, 128.66, 128.53, 128.01, 127.62, 127.52, 126.85, 126.33, 126.25, 126.10, 125.92, 125.21, 122.33, 121.92, 121.80, 121.77, 118.32, 111.63, 46.18, 31.36, 29.90, 26.33, 22.36, 13.90 ppm; elemental analysis (%) calcd for $C_{48}H_{41}F_4IrN_5B$: C 59.70, H 4.25, N 7.26; found: C 59.40, H 4.15, N 6.84; MS (EI): m/z:: 880; found: 880 $[M-BF_4^-]^+$.

General procedures for the synthesis of macroligands, with PFCz as an example: 2,7-Bis(4,4,5,5-tetramethyl-1,3,2-dioxaborolan-2-yl)-9,9-dioctylfluorene (632 mg, 1.0 mmol), 3,6-dibromo-9-(*N*-(2-(pyridin-2-yl)benzimidazole)hexyl)carbazole (602 mg, 1.0 mmol), and tetrakis(triphenylphosphine)palladium (5 mg) were dissolved in toluene/THF (10 mL, 3:1) and stirred for 0.5 h, and then Et_4NOH aqueous solution (20%, 4 mL) was added. The mixture was heated to 100°C and stirred for 2 d under argon. The polymer was then capped by addition of 2-(4,4,5,5-tetramethyl-1,3,2-dioxaborolan-2-yl)-9,9-dioctylfluorene (100 mg), the mixture was stirred for 12 h, and the polymer was then capped with bromobenzene (1 mL), followed by heating for another 12 h. The mixture was poured into stirred methanol (200 mL) to generate plenty of light-yellow precipitates. The solid was collected by filtration and then dissolved in toluene and washed twice with dilute $NaHCO_3$ solution. The careful reprecipitation procedure in acetone/methanol was repeated several times. The polymer was further purified by washing with acetone at reflux in a Soxhlet for 2–3 days. The light-yellow solid was dried under vacuum at room temperature (0.43 g, 52%).

PFCz (yield 52%): ^{1}H NMR (300 MHz, $CDCl_3$): $\delta=8.56$–8.53 (m, 3H), 8.43–8.40 (d, $J=7.9$ Hz, 1H), 7.87–7.74 (m, 10H), 7.51–7.41 (m, 6H) (fluorene ring, carbazole ring, and 2-(pyridin-2-yl)benzimidazole ring), 4.84 (br, 2H; benzimidazole N-CH_2), 4.38 (br, 2H; Cz N-CH_2), 1.92 (m, 4H), 1.69–1.13 (m, 20H), 1.14–0.78 ppm (m, 18H) (aliphatic); ^{13}C NMR (75 MHz, $CDCl_3$): $\delta=151.70$, 150.72, 149.82, 148.60, 142.68, 140.80, 140.34, 139.57, 136.74, 136.60, 133.11, 126.17, 125.60, 124.65, 123.70, 123.62, 123.27, 122.54, 121.64, 120.16, 119.93, 118.99, 110.13, 109.02 (fluorene, carbazole, and 2-(pyridin-2-yl)benzimidazole ring), 68.01, 55.36 (C_9-fluorene ring), 45.27 (Bem N-CH_2), 40.67 (Cz N-CH_2), 31.81, 30.13, 29.92, 29.26, 29.03, 26.95, 26.70, 25.62, 24.01, 22.61, 14.10 ppm (aliphatic); elemental analysis (%) calcd for $C_{59}H_{66}N_4$: C 85.30, H 7.95, N 6.75; found: C 84.62, H 8.14, N 6.05.

PFP (yield 60%): ^{1}H NMR (300 MHz, $CDCl_3$): $\delta=8.65$–8.63 (d, $J=4.7$ Hz, 1H; Py-H), 8.44–8.41 (d, $J=8.0$ Hz, 1H; Py-H), 7.87–7.82 (m, 2H; Py-H), 7.79–7.42 (m, 5H; Ar-H), 7.42–7.14 (m, 8H; Ar-H), 4.84–4.81 (t, $J_1=7.3$ Hz, $J_2=7.1$ Hz, 2H; N-CH_2), 4.0 (br, 2H; OCH_2), 3.80 (br, 3H; OCH_3), 1.91–1.76 (m, 6H), 1.44–1.29 (m, 6H), 1.16–0.91 (m, 21H), 0.83–0.61 ppm (m, 9H); ^{13}C NMR (75 MHz, $CDCl_3$): $\delta=151.16$, 150.76, 150.51, 149.82, 148.59, 142.69, 139.91, 137.07, 136.71, 136.63, 131.68, 128.04, 124.66, 123.60, 123.26, 122.50, 120.13, 119.42, 116.96, 115.52, 110.17, 69.77, 56.84, 55.03 (C_9-fluorene ring), 45.33, 40.60, 32.15, 31.84, 30.28, 30.01, 29.36, 28.93, 26.50, 25.70, 24.13, 22.59, 14.05 ppm; elemental analysis (%) calcd for $C_{54}H_{65}N_3O_2$: C 82.34, H 8.26, N 5.46; found: C 82.33, H 8.33, N 5.01.

General procedures for the preparation of the polymers containing charged iridium complex in their side chains, with PFPIrPiq4 as an example:[19] Polymer PFP (250 mg, 3.178×10^{-4} mol according to repeated units) and tetrakis(1-phenylisoquinoline-*N*,C2′)(μ-chlorobridged)-diiridium(III) (16 mg, 1.27×10^{-5} mol) were dissolved in THF (20 mL). The mixture was heated at reflux under argon for 24 h. As the chelation progressed, the red solid dissolved to form a red clear solution. Excess $NaBF_4^-$ was dissolved in methanol (5 mL) and added dropwise into the reaction mixture. The reaction mixture was kept stirring over a period of 4 h and the resulting solution was concentrated and dropped into methanol to precipitate the polymer. The crude product was washed thoroughly with hot methanol to remove the residual $NaBF_4^-$. The solids were dissolved in toluene and precipitated in hexane again. The desired complex was filtered to produce an orange-red solid, which was washed with methanol in a Soxhlet extractor for 2 d and dried under vacuum at room temperature.

PFPIrPiq2: ^{1}H NMR (300 MHz, $CDCl_3$): $\delta=8.63$ (br), 8.43–8.40 (d), 7.85–7.15 (m), 4.81 (br, N-CH_2), 3.98 (br, OCH_2), 3.80 (br, OCH_3), 1.91–0.81 (m); elemental analysis (%) found: C 82.20, H 7.85, N 5.30; weight-average molecular weight (M_w): 19000 and polydispersity index (PDI): 1.9.

PFPIrPiq4: ^{1}H NMR (300 MHz, $CDCl_3$): $\delta=8.63$ (br), 8.42–8.40 (d), 7.86–7.15 (m), 4.81 (br, N-CH_2), 3.88 (br, OCH_2), 3.80 (br, OCH_3), 1.91–0.81 (m); elemental analysis (%) found: C 80.78, H 7.45, N 5.28; weight-average molecular weight (M_w): 21600 and polydispersity index (PDI): 2.1.

PFPIrPiq10: ^{1}H NMR (300 MHz, $CDCl_3$): $\delta=8.93$ (d), 8.84 (t), 8.63 (br), 8.43–8.40 (d), 8.31–8.28 (d), 8.23–8.21 (d), 7.85–7.15 (m), 6.92–6.89 (d), 6.45–6.43 (d), 4.81 (br, N-CH_2), 3.98 (br, OCH_2), 3.80 (br, OCH_3), 1.91–0.81 (m); elemental analysis (%) found: C 79.79, H 7.45, N 5.48; weight-average molecular weight (M_w): 22000 and polydispersity index (PDI): 1.7.

PFCzIrPiq4: ^{1}H NMR (300 MHz, $CDCl_3$): $\delta=8.54$–8.38 (m), 7.88–7.62 (m), 7.57–7.49 (m), 6.26–6.23 (m), 4.82 (br, benzimidazole N-CH_2), 4.39 (br, Cz N-CH_2), 2.45–2.20 (m), 1.97–0.78 (m, aliphatic); elemental analysis (%) found: C 83.58, H 8.05, N 6.94; weight-average molecular weight (M_w): 5400 and polydispersity index (PDI): 1.6.

PFCzIrPiq10: ^{1}H NMR (300 MHz, $CDCl_3$): $\delta=8.93$ (d), 8.84 (t), 8.54–8.38 (m), 8.31–8.28 (d), 8.23–8.21 (d), 7.88–7.62 (m), 7.57–7.49 (m), 6.92–6.89 (d), 6.45–6.43 (d), 6.26–6.23 (m), 4.82 (br, benzimidazole N-CH_2), 4.39 (br, Cz N-CH_2), 2.45–2.20 (m), 1.97–0.78 (m, aliphatic); elemental analysis (%) found: C 81.58, H 8.01, N 6.85; weight-average molecular weight (M_w): 7300 and polydispersity index (PDI): 1.8.

Device fabrication and characterization: The polymers were dissolved in *p*-xylene and filtered (0.45 mm filter). Patterned glass substrates coated with indium tin oxide (ITO) were cleaned with acetone, detergent, distilled water, and propan-2-ol, and subsequently in an ultrasonic bath. After treatment with oxygen plasma, poly(3,4-ethylenedioxythiophene) (PEDOT) doped with poly(styrenesulfonic acid) (PSS; Batron-P 4083, Bayer AG) (150 nm) was spin-coated onto the ITO substrate, which was followed by drying in a vacuum oven at 80°C for 8 h. A thin film of polymers was spin-coated on top of the PEDOT. The film thicknesses of the active layers were around 75–80 nm, measured with an Alfa Step 500 surface profiler (Tencor). A thin layer of TPBI (50 nm), a layer of Ba (4–5 nm), and a layer of Al (150 nm) were subsequently vacuum-evaporated onto the top of the EL polymer layer under vacuum. Device performance was measured in a dry box. Current–voltage (*I–V*) characteristics were recorded with a Keithley 236 source meter. EL spectra were recorded with an Oriel Instaspec IV CCD Spectrograph. Luminance was measured with a PR 705 photometer (Photo Research). The external quantum efficiencies were determined with a Si photodiode with calibration in an integrating sphere (IS 080, Labsphere).

Acknowledgements

The authors are grateful to the Ministry of Science and Technology of China (No. 2002CB613403) and the National Natural Science Foundation

of China (No.20574021, 50433030, and U0634003) for their financial support.

[1] a) M. A. Baldo, D. F. O'Brien, Y. You, A. Shoustikov, S. Sibley, M. E. Thompson, S. R. Forrest, *Nature* **1998**, *395*, 151–154; b) D. F. O'Brien, M. A. Baldo, M. E. Thompson, S. R. Forrest, *Appl. Phys. Lett.* **1999**, *74*, 442–444; c) C. Adachi, M. A. Baldo, S. R. Forrest, M. E. Thompson, *Appl. Phys. Lett.* **2000**, *77*, 904–906; d) Y. Wang, N. Herron, V. V. Grushin, D. Lecloux, V. Petrov, *Appl. Phys. Lett.* **2001**, *79*, 449–451; e) E. Holder, B. M. W. Langeveld, U. S. Schubert, *Adv. Mater.* **2005**, *17*, 1109–1121; f) T. D. Anthopoulos, M. J. Frampton, E. B. Namdas, P. L. Burn, I. D. W. Samuel, *Adv. Mater.* **2004**, *16*, 557–560; g) X. Gong, M. R. Robison, J. C. Ostrowski, G. C. Bazan, D. Moses, A. J. Heeger, *Adv. Mater.* **2002**, *14*, 581–585.

[2] E. B. Namdas, A. Ruseckas, I. D. W. Samuel, S. Lo, P. L. Burn, *J. Phys. Chem. B* **2004**, *108*, 1570–1577.

[3] a) C. T. Wong, W. K. Chan, *Adv. Mater.* **1999**, *11*, 455–459; b) Z. H. Peng, A. R. Gharavi, L. P. Yu, *J. Am. Chem. Soc.* **1997**, *119*, 4622–4632; c) T. Pautzsch, E. Klemm, *Macromolecules* **2002**, *35*, 1569–1575.

[4] a) C. L. Lee, N. G. Kang, Y. S. Coho, J. S. Lee, J. J. Kim, *Opt. Mater.* **2003**, *21*, 119–123; b) S. Tokito, M. Suzuki, F. Sato, M. Kamachi, K. Shirane, *Org. Electron.* **2003**, *4*, 105–111.

[5] X. Chen, J. L. Liao, Y. Liang, M. O. Ahmed, H. E. Tseng, S. A. Chen, *J. Am. Chem. Soc.* **2003**, *125*, 636–637.

[6] A. J. Sandee, C. K. Williams, N. R. Evans, J. E. Davies, C. E. Boothby, A. Köhler, R. H. Friend, A. B. Holmes, *J. Am. Chem. Soc.* **2004**, *126*, 7041–7048.

[7] a) J. X. Jiang, C. Y. Jiang, W. Yang, H. Y. Zhen, F. Huang, Y. Cao, *Macromolecules* **2005**, *38*, 4072–4081; b) X. Gong, J. C. Ostrowski, G. C. Bazan, D. Moses, A. J. Heeger, M. S. Liu, A. K.-Y. Jen, *Adv. Mater.* **2003**, *15*, 45–49; c) M. Sudhakar, P. I. Djurovich, T. E. Hogen-Esch, M. E. Thompson, *J. Am. Chem. Soc.* **2003**, *125*, 7796–7797; d) N. R. Evans, L. S. Devi, C. S. K. Mak, S. E. Watkins, S. I. Pascu, A. Köhler, R. H. Friend, C. K. Williams, A. B. Holmes, *J. Am. Chem. Soc.* **2006**, *128*, 6647–6656; e) B. W. D′Andrade, R. J. Holmes, S. R. Forrest, *Adv. Mater.* **2004**, *16*, 624–628.

[8] a) H. Y. Zhen, C. Y. Jiang, W. Yang, J. X. Jiang, F. Huang, Y. Cao, *Chem. Eur. J.* **2005**, *11*, 5007–5016; b) H. Y. Zhen, C. Luo, W. Yang, W. Y. Song, B. Du, J. X. Jiang, C. Y. Jiang, Y. Zhang, Y. Cao, *Macromolecules* **2006**, *39*, 1693–1700.

[9] J. D. Slinker, A. A. Gorodetsky, M. S. Lowry, J. Wang, S. Parker, R. Rohl, S. Bernhard, G. G. Malliaras, *J. Am. Chem. Soc.* **2004**, *126*, 2763–2767.

[10] a) Md. K. Nazeeruddin, R. Humphry-Baker, D. Berner, S. Rivier, L. Zuppiroli, M. Graetzel, *J. Am. Chem. Soc.* **2003**, *125*, 8790–8797; b) E. A. Plummer, A.V. Dijken, H. W. Hofstraat, L. D. Cola, K. Brunner, *Adv. Funct. Mater.* **2005**, *15*, 281–289.

[11] a) J. R. Carlise, X. Y. Wang, M. Weck, *Macromolecules* **2005**, *38*, 9000–9008; b) V. Marin, E. Holder, A. R. M. Michael, R. Hoogenboom, U. S. Schubert, *Macromol. Rapid Commun.* **2004**, *25*, 793–799; c) E. Holder, V. Marin, M. A. R. Meier, U. S. Schubert, *Macromol. Rapid Commun.* **2004**, *25*, 1491–1496.

[12] a) S. J. Liu, Q. Zhao, R. F. Chen, Y. Deng, Q. L. Fan, F. Y. Li, L. H. Wang, C. H. Huang, W. Huang, *Chem. Eur. J.* **2006**, *12*, 4351–4352; b) T. Yasuda, T. Yamamoto, *Adv. Mater.* **2003**, *15*, 293–296.

[13] a) S. C. Yu, S. J. Hou, W. K. Chan, Macromolecules **1999**, *32*, 5251–5256; b) D. Knapton, S. J. Rowan, C. Weder, *Macromolecules* **2006**, *39*, 651–657.

[14] C. G. Cameron, T. J. Pittman, P. G. Pickup, *J. Phys. Chem. B* **2001**, *105*, 8838–8844.

[15] F. S. Liang, Q. G. Zhou, Y. X. Cheng, L. X. Wang, D. G. Ma, X. B. Jing, F. S. Wang, *Chem. Mater.* ***2003****, 15*, 1935–1936.

[16] M. Ranger, D. Rondeau, M. Leclerc, *Macromolecules* **1997**, *30*, 7686–7691.

[17] B. Liang, C. Y. Jiang, Z. Chen, X. J. Zhang, H. H. Shi, Y. Cao, *J. Mater. Chem.* **2006**, *16*, 1281–1288.

[18] A. B. Tamayo, S. Garon, T. Sajoto, P. I. Djurovich, I. M. Tsyba, R. Bau, M. E. Thompson, *Inorg. Chem.* **2005**, *44*, 8723–8732.

[19] P. Thomas, K. Elisabeth, T. Pautzsch, E. Klemm, *Macromolecules* **2002**, *35*, 1569–1575.

[20] Y. J. Su, H. L. Huang, C. L. Li, C. H. Chien, Y. T. Tao, P. T. Chou, S. Datta, R. S. Liu, *Adv. Mater.* **2003**, *15*, 884–888.

[21] M. G. Colombo, A. Hauser, H. U. Gudel, *Inorg. Chem.* **1993**, *32*, 3088–3092.

[22] C. J. Xia, R. C. Advincula, *Macromolecules* **2001**, *34*, 5854–5859.

[23] a) J. L. Bredas, R. Silbey, D. S. Boudreaux, R. R. Chance, *J. Am. Chem. Soc.* **1983**, *105*, 6555–6559; b) B. Liu, W. Yu, Y. Lai, W. Huang. *Chem. Mater.* **2001**, 13, 1984–1991; c) J. Pei, X. L. Liu, W. L. Yu, Y. H. Lai, Y. H. Niu, Y. Cao, *Macromolecules* **2002**, 35, 7274–7280.

[24] a) S. Lamansky, P. I. Djurovich, F. Aldel-Razzaq, S. Garon, D. L. Murphy, M. E. Thompson, *J. Appl. Phys.* **2002**, *92*, 1570–1575; b) A. van Dijken, J. J. A. M. Bastiaansen, N. M. M. Kiggen, B. M. W. Langeveld, C. Rothe, A. Monkman, I. Bach, P. Stossel, K. Brunner, *J. Am. Chem. Soc.* **2004**, *126*, 7718–7727.

[25] K. Brunner, A. Dijken, H. Börner, J. J. A. M. Bastiaansen, N. M. M. Kiggen, B. M. W. Langeveld, *J. Am. Chem. Soc.* **2004**, *126*, 6035–6042.

[26] a) S. J. Liu, Q. Zhao, Y. Deng, Y. J. Xia, J. Lin, Q. L. Fan, L. H. Wang, W. Huang, *J. Phys. Chem. C* **2007**,*111*,1166–1175;b) G. Kalyuzhny, M. Buda, J. NcNeill, P. Barbara, A. J. Bard, *J. Am. Chem. Soc.* **2003**, *125*, 6272–6283; c) M. A. Baldo, S. Lamansky, P. E. Burrows, M. E. Thompson, S. R. Forrest, *Appl. Phys. Lett.* **1999**, *75*, 4–6; d) M. A. Baldo, C. Adachi, S. R. Forrest, *Phys. Rev. B* **2000**, *62*, 10967–10977; e) J. Kalinowski, W. Stampor, M. Cocchi, D. Virgili, V. Fattori, P. D. Marco, *Phys. Rev. B* **2002**, *66*, 235321.

[27] X. H. Yang, D. Neher, D. Hertel, T. K. Däubler, *Adv. Mater.* **2004**, *16*, 161–165.

[28] a) J. D. Slinker, D. Bernards, P. L. Houston, H. Abruna, S. Bernhard, G. G. Malliaras, *Chem. Commun.* **2003**, 2392–2399; b) Q. B. Pei, G. Yu, C. Zhang, Y. Yang, A. J. Heeger, *Science* **1995**, *269*, 1086–1088; c) Q. B. Pei, Y. Yang, G. Yu, C. Zhang, A. J. Heeger, *J. Am. Chem. Soc.* **1996**, *118*, 3922–3929.

[29] E. Itoh, T. Yamashita, K. Miyairi, *J. Appl. Phys.* **2002**, *92*, 5971–5976.

Received: December 17, 2006
Revised: April 4, 2007
Published online: June 21, 2007

